

COMPARISON OF IMAGE-BASED FUNCTIONAL MONITORING THROUGH RESAMPLING AND COMPRESSION

Steven J. Simske, Margaret Sturgill, Jason S. Aronoff

Hewlett-Packard Labs, 3404 E. Harmony Rd. MS 36, Fort Collins CO USA 80528

Contact: Steven.Simske@hp.com

1. INTRODUCTION

Image-based applications such as remote surveillance and environmental monitoring are often bandwidth-limited, and benefit from image down-sampling or compression. Often a decision is made without considering the relative impact on the functional goal of the monitoring of the different down-sampling and/or compression choices. In this paper, we use a specific “remote” monitoring application—the distinction between images of authentic products and counterfeit products—to assess the impact of down-sampling and compression on the classification accuracy of the counterfeit detection imaging software.

2. EXPERIMENTS PERFORMED

We obtained original packages for 10 authentic and 10 counterfeit HP inkjet cartridges. Five different types of images were each scanned at 600x600 dots/inch (dpi) horizontal x vertical resolution using a desktop (HP Scanjet 8200), as shown in Figure 1. These are a set of two barcodes (hereafter “Barcode”), a blue spot color region (“Blue”), a set of color targets for print quality assurance (“Color”), a set of five branding images separated by whitespace (“Images”) and a single large image (“Meadow”). The image areas were approximately 2.7, 2.8, 2.3, 4.2 and 10.1 in², respectively.

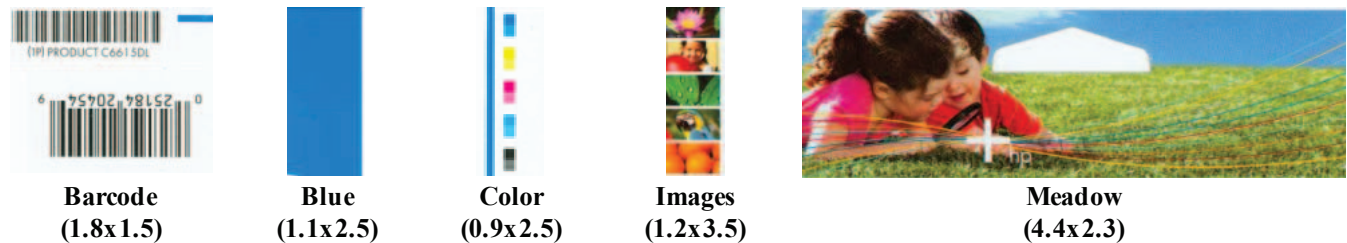


Figure 1. Samples of each of the five image types (actual image sizes in inch x inch at 600 dpi in parentheses)

Ten image processing measurements, or “features” were computed for each of these 100 images (5 each from the 10 authentic and 10 counterfeit packages). Image entropy (“ e ”) and standard deviation of the image histogram (“ $\text{Std}(H_1)$ ”), were computed from the intensities of the individual pixels, p_k , as shown below. Other metrics computed were the percent of pixels with larges relative neighborhood variance (“ $\%Edges$ ”), the mean value for these edges (“ μ_{Edge} ”), and the mean pixel variance, PV_{xy} , based on the local differences in pixel intensity (compared to the four nearest pixels not in the same row or column).

$$e = -\sum_{k=0}^{255} \frac{p_k}{\sum_{k=0}^{255} p_k} * \ln \left(\frac{p_k}{\sum_{k=0}^{255} p_k} \right)$$

$$\text{Std}(H_1) = \frac{\sum_{k=0}^{255} p_k * (k - \mu)^2}{\sum_{k=0}^{255} p_k}$$

Mean saturation (“ μ_{Sat} ”) was then computed, where saturation is defined as $255 * (1 - \min(R, G, B)) / (R + G + B)$. Mean connected component region size and variance were computed after thresholding the images based on pixel intensity (“ $\mu_{Size-Intensity}$ ” and “ $\mu_{Size-Intensity-\sigma^*}$ ”, respectively) and based on saturation (“ $\mu_{Size-Saturation}$ ” and “ $\mu_{Size-Saturation-\sigma^*}$ ”, respectively). These metrics were also computed for the same images down-sampled using ImageMagick [1] “-resample” option to 10 (Images, Meadow only), 20, 30, 40, 50, 60, 75, 100, 150, 200 and 300 dpi vertical x horizontal resolution; and for images compressed using JPEG to 1% or 2% original image size (effectively 60 and 85 dpi, respectively) before and after (effectively 30 and 42 dpi, respectively) down-sampling to 300 dpi.

3. RESULTS

The five different types of images varied greatly by image metric. Seven of the metrics (e , $\text{Std}(\mathbf{H}_1)$, $\%Edges$, $\mu_{\text{Size-Intensity}}$, $\mu_{\text{Size-Intensity}-\sigma^*}$, $\mu_{\text{Size-Saturation}}$, and $\mu_{\text{Size-Saturation}-\sigma^*}$) distinguished the “Images” and “Meadow” classes from the other 3 classes, and $\mu_{\text{Size-Saturation}-\sigma^*}$ distinguishes the class “Images” from the class “Meadow”. The metrics PV_{xy} and μ_{sat} provide assignment of the remaining images to the “Barcode”, “Blue” and “Colors” classes. Thus, a decision tree was used to assign each original image to one of these five types based on one or more of these 10 “predictive” metrics. A previously described classifier [2] was then used to identify “authentic” and “counterfeit” images for each of these five image types. Each metric is assigned a critical point (CPT) to one side of which it is assigned to “authentic” and the other to “counterfeit”.

Previous work [3,4,5] has shown that statistical image metrics can predict image degradation and also be used to grade the quality of image restoration. We applied this approach herein to assess the functional metric of correctly assigning an image to “counterfeit” or “authentic”. The binary classifier [2] provides a comparative metric for accuracy, the statistical confidence at the critical point (α_{CPT}), which was used to determine the “functional monitoring” capability of the down-sampled images. That is, for each metric, and for the mean of all 10 metrics (as described in [2]), we computed α_{CPT} and compared it to the α_{CPT} for the original 600 dpi images. If α_{CPT} for the down-sampled or compressed images $\geq \alpha_{\text{CPT}}$ for the 600 dpi original images, then we are better off transmitting the smaller images. For the mean of all ten metrics, the α_{CPT} was .896, 0.708, 0.788, 0.816 and 0.743 (i.e. between 70%-90% accuracy) for Barcode, Blue, Color, Images and Meadow types, respectively. The overall classification accuracy (using the binary classifier and all ten metrics) was 100% for all image sizes of the Barcode, Images and Meadow classes sizes; for the Color class image sizes from 30-600 dpi and when compressed from the 600 dpi original; and for the image sizes 40, 50, 75, 300 and 600 dpi for the Blue class. So, the classifier [2] was, in general, quite capable at differentiating authentic from counterfeit images.

We then defined the $@A_{\text{TF}}$, or at-accuracy throughput factor, as the relative number of images (compared to 1 at 600 dpi) that can be successfully assigned to “counterfeit” or “authentic” classes with an accuracy \geq the accuracy obtained for the original 600 dpi images, while using the same overall size in memory. For down-sampling, $@A_{\text{TF}}$ was 1, 4, 9, 900 and 3600, respectively, for the Barcode, Blue, Color, Images and Meadow image types. For compression, only the Blue and Meadow classes had a $@A_{\text{TF}}$ value greater than 1: specifically, 100 for the Blue images compressed from 600 dpi originals, and 400 for the Meadow class since all four compression approaches resulted in α_{CPT} greater than at 600 dpi.

4. DISCUSSION AND CONCLUSIONS

Our results support the following approach to remote functional monitoring: (1) classify the image; (2) determine the smallest image (either down-sampled or compressed) for which α_{CPT} is \geq to α_{CPT} for the 600 dpi original image; (3) transmit this smaller image; and (4) perform functional monitoring (in this case, correctly classifying each image). In this way, we achieved a higher overall accuracy by sending the Barcode images unaltered; compressing the Blue images by a factor of 100; and down-sampling the Color, Images and Meadow images by factors of 9, 900 and 3600, respectively. This overall system results in an effective $@A_{\text{TF}}$ of 4.45; that is, improved accuracy is achieved with a 4.45 reduction in transmission bandwidth.

In addition to remote surveillance and environmental monitoring, the techniques described here can be used to determine image down-sampling or compression recommendations for other “functional monitoring” product authentication/counterfeit detection. Since the classification of images is functional—that is, dependent on the task at hand—we believe a consideration of whether to down-sample or compress (and by what factor) should be an important part of any image-based monitoring application. Thanks to Dave Kellar and George Guillory for authentic and counterfeit packages.

6. REFERENCES

- [1] ImageMagick, <http://www.imagemagick.org/script/index.php>.
- [2] S. J. Simske, “Low-resolution photo/drawing classification: metrics, method and archiving optimization,” *Proceedings IEEE ICIP*, IEEE, Genoa, Italy, pp. 534-537, 2005.
- [3] D. Li and S.J. Simske, “Atmospheric turbulence degraded image restoration by kurtosis minimization,” *IEEE Geoscience and Remote Sensing Letters*, IEEE, Vol. 6, in press, 2009.
- [4] D. Li, R.M. Mersereau and S.J. Simske, “Atmospheric turbulence degraded image restoration using principal components analysis,” *IEEE Geoscience and Remote Sensing Letters*, IEEE, Vol. 4, No. 3, pp. 340-344, 2007.
- [5] D. Li, R.M. Mersereau and S.J. Simske, “Blur identification based on kurtosis minimization,” *Proceedings IEEE ICIP*, IEEE, Genoa, Italy, pp. 905-908, 2005.